Biochemistry

Article

Cite This: *Biochemistry* 2019, 58, 5339−5350

pubs.acs.org/biochemistry

Crystal Structures of L-DOPA Dioxygenase from *Streptomyces sclerotialus*

Yifan Wang,[†] Inchul Shin,[†] Yizhi Fu,[‡] Keri L. Colabroy,*[,‡] and Aimin Liu*[,†]

[†]Department of Chemistry, University of Texas at San Antonio, San Antonio, Texas 78249, United States

[‡]Department of Chemistry, Muhlenberg College, Allentown, Pennsylvania 18104, United States

Supporting Information

ABSTRACT: Extradiol dioxygenases are essential biocatalysts for breaking down catechols. The vicinal oxygen chelate (VOC) superfamily contains a large number of extradiol dioxygenases, most of which are found as part of catabolic pathways degrading a variety of natural and human-made aromatic rings. The L-3,4-dihydroxyphenylalanine (L-DOPA) extradiol dioxygenases compose a multitude of pathways that produce various antibacterial or antitumor natural products. The structural features of these dioxygenases are anticipated to be distinct from those of other VOC extradiol dioxygenases. Herein, we identified a new L-DOPA dioxygenase from the thermophilic bacterium *Streptomyces sclerotialus* (SsDDO) through a sequence and genome context analysis. The activity of SsDDO was kinetically characterized with L-DOPA using an ultraviolet−visible spectrophotometer and an oxygen electrode. The optimal temperature of the assay was 55 °C, at which the K_m and k_{cat} of SsDDO were 110 ± 10 μM and 2.0 ± 0.1 s^{-1}, respectively. We determined the *de novo* crystal structures of SsDDO in the ligand-free form and as a substrate-bound complex, refined to 1.99 and 2.31 Å resolution, respectively. These structures reveal that SsDDO possesses a form IV arrangement of $\beta\alpha\beta\beta\beta$ modules, the first characterization of this assembly from among the VOC/type I extradiol dioxygenase protein family. Electron paramagnetic resonance spectra of Fe−NO adducts for the resting and substrate-bound enzyme were obtained. This work contributes to our understanding of a growing class of topologically distinct VOC dioxygenases, and the obtained structural features will improve our understanding of the extradiol cleavage reaction within the VOC superfamily.

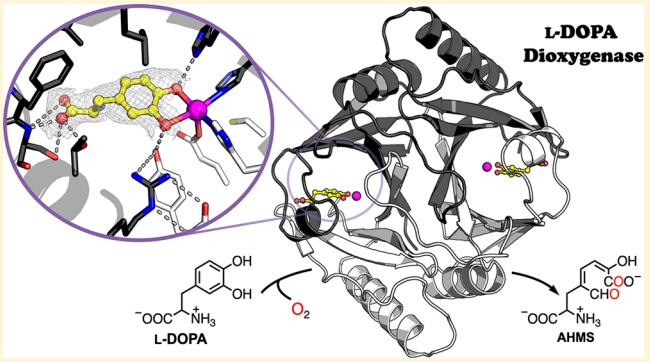

Dioxygenase chemistry is essential for catechol breakdown. The largest natural source of catechols, or 1,2-dihydroxybenzenes, is the plant woody-tissue polymer, lignin. Lignin is a polymer of catecholic monomers that strengthens the cell walls of a plant but impedes access to the cellulosic sugars used in biofuel production.[1,2] It is also a relatively untapped source of carbon that could be repurposed and valorized into feedstocks and natural products.[3] Ever since the first example of a "pyrocatechase" (catechol-1,2-dioxygenase) was discovered 70 years ago,[4] numerous catechol dioxygenases from all domains of life and in all types of metabolic pathways have been reported, including those that use molecular oxygen to break the aromatic ring adjacent to the diol, generating an aldehyde and a carboxylic acid at either end of the six-carbon chain. These enzymes were the inaugural members of two functional classes of oxygenases: the intradiol and the extradiol dioxygenases.[5] When found in degradation pathways, the extradiol dioxygenase reactions linearize the catecholic substrates such that downstream products can enter central metabolism.[5] In some cases, the linearized products undergo cyclization and further derivatization to yield a natural product.[6−8]

The extradiol cleavage reaction has been adapted to the structural scaffolds of three distinct superfamilies: vicinal oxygen chelate (VOC or type I),[9] LigAB (type II),[10] and cupin (type III).[11] VOC/type I dioxygenases are the best characterized group of extradiol dioxygenases, and they are mostly found as part of catabolic pathways degrading a variety of natural and synthetic aromatic compounds. All VOC superfamily members use a metal center to coordinate an organic substrate, intermediate, or transition state through both of its vicinal oxygen atoms;[9] for example, the neighboring hydroxyl groups of catechol are typically chelated by an active site Fe^{2+} in the VOC/type I extradiol dioxygenases.[12] Despite significant knowledge of VOC structure, domain architecture, and enzymatic function, the relationships between VOC domain architecture and function remain complex and poorly understood.[13] While the chemistry throughout the VOC

Special Issue: Current Topics in Mechanistic Enzymology 2019

Received: May 2, 2019
Revised: June 7, 2019
Published: June 10, 2019

DOI: 10.1021/acs.biochem.9b00396
Biochemistry 2019, 58, 5339−5350

Scheme 1. Biosynthesis Pathway of Pyrroline Carboxylic Acid, in which SsDDO Catalyzes the Second Step, L-DOPA Dioxygenation[a]

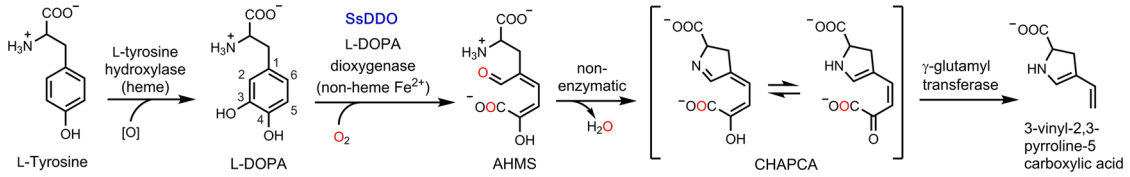

[a]The functionalized pyrroline carboxylic acid is further modified and incorporated into the natural product scaffold.

superfamily varies, each superfamily member is structurally defined as an assembly of $\beta\alpha\beta\beta\beta$ modules.[9] The connectivity of these $\beta\alpha\beta\beta\beta$ modules is permuted across the superfamily into six different topologies [forms I–VI (Figure S1)].[9,14] The functional class of nonredox VOC enzymes contains representative domain architectures of every possible assembly, with the exception of monomeric form II. However, among the six possible domain architectures, nearly every characterized VOC/type I extradiol dioxygenase is of form V architecture, which is a four-module monomer of two back-to-back stacked domains.[9]

The first L-DOPA extradiol dioxygenase, LmbB1, was identified almost 25 years ago from the biosynthetic gene cluster of lincomycin from *Streptomyces lincolnensis*.[15−17] Later, several of its homologues from other bacterial sources were characterized.[18] These dioxygenases are involved in the biosynthesis of antibacterial or antitumor natural products, such as HrmF of hormaomycin,[19] SibV of anthramycin,[20,21] Por13 of porothramycin,[22] SibV of sibiromycin,[23] and TomH of tomaymycin.[24] L-DOPA dioxygenases employ a ferrous iron to catalyze the insertion of dioxygen into the aromatic ring of L-DOPA, linearizing it to the chromophoric 5-alanyl-2-hydroxymuconate 6-semialdehyde (AHMS), which undergoes a prompt, non-enzymatic cyclization to 3-carboxy-3-hydroxyallylidene-3,4-dihydropyrrole-2-carboxylic acid (CHAPCA) (Scheme 1).[25] L-DOPA dioxygenases were labeled as one-domain VOC enzymes based only on the length of sequence and homology to VOC family enzymes.[5] These one-domain VOC dioxygenases were in contrast to the larger (>40 kDa), well-studied, two-domain/form V enzymes, such as catechol 2,3-dioxygenase (C23O), 2,3-dihydroxybiphenyl 1,2-dioxygenase (DHBD), and homoprotocatechuate 3,4-dioxygenase (HPCD).[5] While the smaller VOC dioxygenases, typified by L-DOPA dioxygenases, have been studied biochemically, no detailed structural information has been available to date.

Here, we identify a new L-DOPA extradiol dioxygenase from a thermophilic bacterium *Streptomyces sclerotialus* (SsDDO) by sequence and genome context analysis. Moreover, the first three-dimensional structural study of an L-DOPA dioxygenase was completed by X-ray crystallography. A temperature-dependent activity assay was performed by monitoring the product chromophore to investigate the optimal temperature for catalysis. The iron center was also characterized by electron paramagnetic resonance (EPR) spectroscopy. These results demonstrate that SsDDO is the inaugural member of a new class of topologically distinct VOC dioxygenases, whose structure and mechanism will improve our understanding of the extradiol cleavage reaction.

MATERIALS AND METHODS

Protein Overexpression and Purification. The synthetic gene of the codon-optimized SsDDO in the pET28a expression vector was purchased from GenScript. The *Escherichia coli* BL21 (DE3) cells (Merck) containing the expression plasmid for N-terminally His_6-tagged SsDDO were cultured in Luria-Bertani medium with kanamycin (50 μg/mL) at 37 °C. When the OD_{600} reached 0.6 AU, the temperature was decreased to 20 °C and isopropyl β-thiogalactopyranoside and ferrous ammonium sulfate were added to final concentrations of 600 and 50 μM, respectively. The cells were harvested after 18 h and resuspended in buffer A [50 mM Tris-HCl and 200 mM NaCl (pH 8.0)]. An LM20 cell disruptor (Microfluidics) was used to lyse cells, and the supernatant was recovered after centrifugation (25000×*g* for 40 min at 4 °C).

The protein was then purified by affinity chromatography using a HisTrap column (GE Healthcare) with a gradient of buffer B [50 mM Tris-HCl, 200 mM NaCl, and 500 mM imidazole (pH 8.0)]. The eluted protein was concentrated using an Amicon centrifugal filter with a 3 kDa cutoff (Millipore) and desalted into 50 mM Tris-HCl and 50 mM NaCl (pH 8.0) for further use.

For structural studies, seleno-L-methionine (SeMet)-substituted protein was cultured in M9 minimal medium with the addition of 0.25 mM SeMet according to the published method.[26] The purification procedure was the same as the aforementioned wild-type SsDDO. The eluted SsDDO was then treated with a Thrombin CleanCleave Kit (Sigma) to remove the His tag. The untagged protein was further purified again with a HisTrap column and followed by a Superdex-75 column (GE Healthcare) equilibrated with 50 mM Tris-HCl (pH 7.4).

Temperature-Dependent L-DOPA Dioxygenase Activity Assay. SsDDO was freshly prepared by anaerobic iron reconstitution prior to an activity assay using a published method.[27] Apo-SsDDO was prepared by overnight incubation with EDTA (10 mM, pH 8) at 4 °C, followed by desalting to remove EDTA. Fe(II)-SsDDO was prepared by incubating degassed apo-SsDDO with 10 equiv of O_2-free ammonium ferrous sulfate in a glovebox for 30 min, and finally, iron ions were removed by desalting using an argon-saturated buffer. After iron reconstitution, the iron occupancy in SsDDO was around 95%, as assessed by a ferrozine assay.[28] The steady-state kinetic parameters were evaluated on the basis of Fe(II)-SsDDO concentrations. Michaelis–Menten steady-state constants were obtained by reacting SsDDO (0.2–0.5 μM) with L-DOPA (25 μM to 1 mM) in reaction buffer [50 mM potassium phosphate (pH 8.0)]. An Aligent 8453 ultraviolet–visible (UV–vis) spectrophotometer with a temperature-regulated cuvette holder was used to detect the resulting cyclized product of AHMS, CHAPCA, at 414 nm with an extinction coefficient of 47500 M^{-1} cm^{-1}.[16] The temperature was adjusted to 25, 40, 50, 55, 60, and 65 °C to determine the optimal temperature of the assay. An oxygen electrode

DOI: 10.1021/acs.biochem.9b00396
Biochemistry 2019, 58, 5339−5350

(Oxygraph, Hansatech Instruments) was used to measure oxygen consumption under the same conditions. Initial rates were measured and plotted versus L-DOPA concentration and fit with the Michaelis−Menten equation using standard nonlinear regression (Origin 8.5, Microcal).

Crystallization. The untagged protein was concentrated to 10−15 mg/mL and mixed at a 1:1 volume ratio with a crystallization buffer of 0.1 M Tris-HCl (pH 8.5), 0.2 M $MgCl_2$, and 16% (w/v) PEG 8000 using the hanging drop, vapor-diffusion method at 295 K. Microcrystals formed the next day and grew to an optimal size suitable for X-ray diffraction after 3−4 days. Crystals were cryoprotected with crystallization buffer containing an additional 20% (v/v) glycerol and then flash-cooled in liquid nitrogen. For substrate-bound crystals, crystallization trays were set up inside a glovebox with an argon-saturated protein solution and crystallization buffer. After anaerobic crystals were formed, the ES complex was prepared by soaking the crystals with 5 mM L-DOPA under a strictly anaerobic condition for half an hour before they were rapidly cooled in liquid nitrogen.

Data Collection and Structure Determination. All data were collected at 100 K and processed using HKL2000.[29] Single-wavelength anomalous diffraction data for the SeMet-substituted SsDDO were collected from beamline SSRL 9-2, and a 2.40 Å resolution data set was obtained at a wavelength of 0.97913 Å, corresponding to an absorption peak of selenium. PHENIX.AutoSol[30] and PHENIX.AutoBuild[31] were used for phasing and model building. A SsDDO structure was also collected at beamline SSRL 9-2 with a resolution of 1.99 Å, which was later termed an initial model for molecular model building and refinement for other structures using PHENIX[32] software packages. The ES complex (SsDDO in complex with L-DOPA) structure of 2.31 Å resolution was collected at SBC 19BM. The E only and ES complex SsDDO original data sets have a strong anisotropic problem; therefore, original data were truncated using an online server.[33] All of the data collection and refinement statistics are summarized in Table 1.

Preparation and EPR Measurement of Nitrosyl Complexes. The preparation of nitrosyl samples and the X-band EPR setup were described previously.[34] Argon-saturated SsDDO (500 μM) was reduced by 5 mM sodium ascorbate for 30 min anaerobically. A slight excess of NONOate (Cayman) was added to reduced SsDDO forming the E-NO$^\bullet$ complex. L-DOPA (5 mM) was then added to generate the ES-NO$^\bullet$ complex. Spectra for high-spin signals were collected at 6 K and 0.796 mW with a 6 G modulation amplitude with a 100 kHz modulation frequency, while spectra for the low-spin dinitrosyl complex were collected at 50 K and 0.05 mW. All spectra were the average of four scans.

RESULTS AND DISCUSSION

Identification of SsDDO as a Putative L-DOPA Dioxygenase. Previous work on L-DOPA dioxygenases, LmbB1, Orf12, and SibV, reported the enzyme existed in purified form as a dimer of identical subunits,[17,21] implying a topology distinct from that of existing, structurally characterized, two-domain VOC/type I dioxygenases. However, further structural study has been impeded due to the failures in the crystallization of LmbB1 and reported homologues; therefore, sequence and genome context were analyzed from a variety of organisms to identify homologues of L-DOPA dioxygenase that would be more amenable to crystallographic study.

Table 1. X-Ray Data Collection and Refinement Statistics

	SeMet SsDDO	SsDDO (E only)	SsDDO (ES complex)
	SAD	single wavelength	single wavelength
Protein Data Bank entry		6ON1	6ON3
	Data Collection[a]		
beamline station	SSRL 9-2	SSRL 9-2	SBC 19BM
wavelength (Å)	0.97913	0.97946	0.97933
space group	$P2_1$	$P2_1$	$P2_1$
cell dimensions			
a, *b*, *c* (Å)	100.1, 46.2, 130.8	100.0, 45.2, 131.2	99.8, 40.7, 128.4
α, β, γ (deg)	90, 106, 90	90, 105, 90	90, 105, 90
resolution (Å)	50−2.40 (2.44−2.40)	50−1.99 (2.02−1.99)	50−2.31 (2.35−2.31)
total no. of reflections	498715	510762	193367
no. of unique reflections	41737	76745	42332
redundancy	11.9 (8.2)	6.7 (6.2)	4.6 (3.8)
R_{merge}[b] (%)	18.7 (92.8)	9.1 (36.5)	12.4 (55.2)
$I/\sigma I$	15.80 (1.04)	20.93 (3.86)	12.0 (1.17)
completeness (%)	91.0 (66.9)	96.9 (91.1)	94.5 (82.0)
$CC_{1/2}$, highest-resolution shell	0.74	0.97	0.83
FOM[c]	0.345		
	Refinement		
resolution (Å)		30.33−1.99	44.01−2.31
no. of reflections		76545	32257
R_{work}[d]/R_{free}[e]		20.7/25.6	23.5/29.4
no. of atoms			
protein		7190	7246
iron		6	6
ligand		N/A	84
solvent		376	342
B-factor (Å^2)			
protein		46.86	32.04
iron		34.98	33.14
ligand		N/A	32.7
solvent		47.41	31.07
root-mean-square deviation			
bond lengths (Å)		0.006	0.002
bond angles (deg)		0.769	0.498
Ramachandran analysis (%)			
favored		98.46	96.05
allowed		1.18	3.37
outlier[f]		0.35	0.58

[a]Numbers in parentheses refer to data in the highest-resolution shell. [b]$R_{merge} = \sum|I_h - \langle I_h\rangle|/\sum I_h$, where I_h is the observed intensity and $\langle I_h\rangle$ is the average intensity. [c]Figure of merit after RESOLVE.[15,16] [d]$R_{work} = \sum||F_o| - k|F_c||/\sum|F_o|$. [e]$R_{free}$ is the same as R_{obs} for a selected subset (10%) of the reflections that was not included in prior refinement calculations. [f]Outliers are from the surface flexible region, which are irrelevant to substrate binding. Total of three outliers in the E only structure: Ala85 in chain B and Ala79 and Asp81 in chain C. Total of five outliers in the ES structure: Pro159 in chain B, chain D, and chain F, Leu27 in chain E, and Ala14 in chain F.

DOI: 10.1021/acs.biochem.9b00396
Biochemistry 2019, 58, 5339−5350

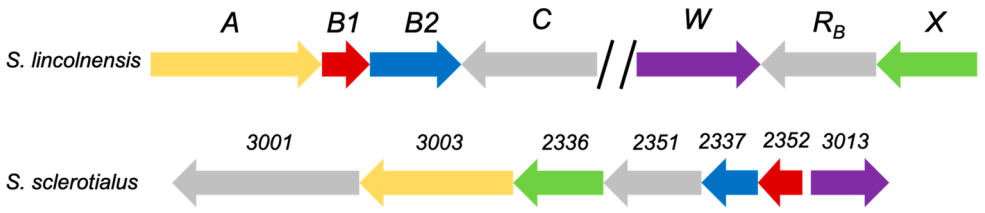

Assigned/annotated function	*S. lincolnensis* gene (protein)	*S. sclerotialus* gene (protein)
γ-glutyltransferase	*lmbA* (CAA55746)	*3003* (WP_030623003)
L-DOPA dioxygenase	*lmbB1* (CAA55747)	*2352* (WP_051872352)
L-tyrosine hydroxylase	*lmbB2* (CAA55748)	*2337* (WP_051872337)
O-methyltransferase	*lmbW* (CAA55769)	*3013* (WP_030623013)
PhzF phenazine biosynthetic protein	*lmbX* (CAA55771)	*2336* (WP_051872336)

Figure 1. Identification of SsDDO as a putative L-DOPA dioxygenase through a genome context analysis of the biosynthetic gene cluster of pyrroline carboxylic acid in *S. lincolnensis* and *S. sclerotialus*. L-Tyrosine hydroxylases (blue): *lmbB2* and 2337. L-DOPA dioxygenases (red): *lmbB1* and 2352. γ-Glutamyltransferase-like C−C bond hydrolases (yellow): *lmbA* and 3003. *O*-Methyltransferase (purple): *lmbW* and 3013. PhzF phenazine biosynthetic protein/unknown function (green): *lmbX* and 2336.

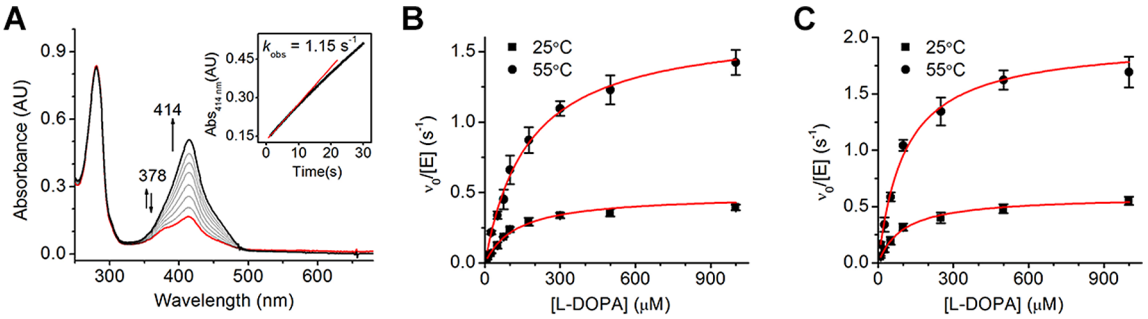

Figure 2. (A) UV−vis spectra of the SsDDO-catalyzed reaction. The transient linearized product (AHMS; λ_{max} = 378 nm) immediately cyclizes to CHAPCA with a λ_{max} of 414 nm. The reaction was performed with 0.2 μM enzyme with 0.5 mM L-DOPA at 55 °C. Initial rate k_{obs} = 1.15 s^{-1} (inset). Steady-state kinetic assay of SsDDO with L-DOPA at 25 and 55 °C, obtained using UV−vis spectrometer (B) and oxygen electrode (C), respectively. The data were fit to the Michaelis−Menten equation shown with red lines.

Genome context analysis was made possible because the extradiol cleavage of L-DOPA was first proposed within the context of a biosynthetic pathway to C_2- or C_3-proline units of several natural products.[35] In fact, the pathways to lincomycin, hormaomycin, and the pyrrolobenzodiazepines of anthramycin, sibiromycin, porothramycin, and tomaymycin have at least three genes in common.[18] L-Tyrosine hydroxylases, L-DOPA dioxygenases, and γ-glutamyltransferase-like N-terminal hydrolases that catalyze C−C bond cleavage are present in all six gene clusters that produce 4-alkyl-L-(dehydro)proline synthons for incorporation into natural products (Scheme 1).[36] When found co-located on the bacterial chromosome, these genes are indicative of a minipathway to a 4-alkyl-L-(dehydro)proline synthon. We identified such a pathway in the organism *S. sclerotialus* ISP-5269, a species first described from an Indian hot spring[37] and later sequenced as part of a genome mining project.[38] The L-DOPA dioxygenase homologue from *S. sclerotialus* is 54% identical to LmbB1 from *S. lincolnensis*, and it clusters on the chromosome with homologues of L-tyrosine hydroxylase (*S. lincolnensis*, LmbB2), the γ-glutamyltransferase (*S. lincolnensis*, LmbA), an *O*-methyltransferase (*S. lincolnensis*, LmbW), and a protein of unknown function (*S. lincolnensis*, LmbX) (Figure 1).

A bioinformatics utility EFI-EST (https://efi.igb.illinois.edu/efi-est/) was employed to generate the enzyme sequence similarity network (SSN)[39] of L-DOPA dioxygenases (Figure S3), and 65 proteins (as of February 2019) were found to be similar with L-DOPA dioxygenases in the UniProt database. At an *e* value of 10^{-55}, this new class of VOC dioxygenases, including LmbB1, Ant12, HrmF, Orf12, Por13, SibV, and TomH, is spread over several smaller clusters. The biosynthetic function of the L-DOPA dioxygenases might be the reason why this homologous group of extradiol dioxygenases is quite distinct from other proteins in primary sequence, or this result could be further evidence of the difficulty in aligning the primary sequence within a superfamily where the essential βαββββ modules can be coupled in frame or inverted with respect to their primary sequence.[13] Nevertheless, all of the resulting proteins are similar in size, and most are annotated as dioxygenases, such as catechol extradiol dioxygenases. Furthermore, the SSN also includes annotations of glyoxalase I-type enzymes, another member of the vicinal oxygen chelate superfamily. The genomic context and the sequence similarity of the SsDDO validated its identity, and the thermophilic nature of the source organism indicated this homologue was likely more amenable to crystallographic study. Consequently, the gene encoding SsDDO was codon-optimized, synthesized, cloned, and expressed in *E. coli* a an ∼20 kDa protein that cleaved L-DOPA.

DOI: 10.1021/acs.biochem.9b00396
Biochemistry 2019, 58, 5339−5350

Catalytic Activity of SsDDO. The optimal temperature of the Fe(II)-SsDDO activity assay was determined by monitoring the formation of its cyclized product, CHAPCA, whose extinction coefficient at 414 nm is 47500 M^{-1} cm^{-1} at pH 8.[16] The transient, linearized product AHMS (λ_{max} = 378 nm) immediately cyclizes to form CHAPCA (Scheme 1 and Figure 2A). The cyclization rate of AHMS is related to the substrate concentration, reaction temperature, pH, and other factors. Therefore, consistent with previous observations of LmbB1,[25] both enzyme-catalyzed cleavage and product cyclization affect the observed activity of SsDDO, and the rate of cyclized product formation is employed to reflect the enzymatic activity. Herein, K_M' and k_{cat}' indicate the observed activity of forming CHAPCA, which are distinct from the steady-state kinetic parameters. Via measurement of the specific activity at various temperatures, the enzymatic activity was observed to increase from 25 to 55 °C, with a decrease in activity when the temperature exceeded 55 °C (Figure S2). Alternatively, steady-state kinetic parameters can also be evaluated by oxygen consumption. Therefore, the oxygen electrode method was employed to measure K_M and k_{cat} at both 25 and 55 °C (Figure 2C and Table 2). The results suggest the K_M obtained with an oxygen electrode is comparable with the K_M' obtained by the UV−vis spectrophotometer while the k_{cat} is slightly higher than k_{cat}'. This is an expected result considering product cyclization was involved in measuring K_M' and k_{cat}', and the non-enzymatic cyclization is not the rate-limiting step or competitive with respect to the enzymatic reaction. Approximately 70% of the rate of dioxygenation activity at 55 °C (both k_{cat}'/K_M' and k_{cat}/K_M) was lost at room temperature (Figure 2B and Table 2).

Table 2. Steady-State Kinetic Parameters for the Reaction of SsDDO with L-DOPA at 25 and 55 °C[a]

temperature (°C)	K_M' (μM)	k_{cat}' (s^{-1})	k_{cat}'/K_M' ($\times 10^3$ s^{-1} M^{-1})
25	130 ± 20	0.48 ± 0.04	3.8 ± 0.6
55	130 ± 20	1.5 ± 0.1	12 ± 2
temperature (°C)	K_M (μM)	k_{cat} (s^{-1})	k_{cat}/K_M ($\times 10^3$ s^{-1} M^{-1})
25	99 ± 6	0.59 ± 0.01	6.0 ± 0.4
55	110 ± 10	2.0 ± 0.1	18 ± 2

[a]The results were obtained using a UV−vis spectrophotometer (top) and an oxygen electrode (bottom).

A kinetic study was previously reported for a SsDDO homologue, LmbB1, the L-DOPA dioxygenase from *S. lincolnensis*. Although the reported K_M' for LmbB1 with L-DOPA (30 μM) was lower than that of SsDDO, the k_{cat}'/K_M' value of 2.3 × 10^3 M^{-1} s^{-1} around room temperature is comparable with the measured values for SsDDO.[25] The temperature-dependent activity of a keratinase from the same thermophilic strain, *S. sclerotialus*, was previously studied, and the corresponding keratinase had a temperature-dependent activity tendency similar to that of SsDDO with a maximum activity that was also at 55 °C.[37]

Global Structure of SsDDO. In solution, LmbB1, Orf12, and SibV have been reported to exist as dimers,[17,21] and their small size (~20 kDa) was termed "one-domain" with respect to other known VOC extradiol dioxygenases, such as the ~40 kDa, two-domain catechol 2,3-dioxygenase.[5] These differences implied a distinct three-dimensional structure for L-DOPA dioxygenase; however, no additional structural investigations were available to understand how the topological arrangement of the protein is accomplished with a one-domain sequence. To provide the first three-dimensional view of this group of dioxygenases, we determined the resting-state crystal structure of SsDDO by single-wavelength anomalous diffraction (SAD) X-ray crystallography and refined it to 1.99 Å resolution. The diffraction data solution was achieved in space group $P2_1$, and three dimers were found in an asymmetric unit. The monomeric SsDDO is composed of three α-helices and eight β-strands, which fold into two structural domains (residues 13−78 and residues 92−160) connected by an intervening segment (residues 79−91) (Figure 3A), and the helices and β-strands are organized into two functional modules with a repeated $\beta\alpha\beta\beta\beta$ pattern ($\beta1-\alpha1-\beta2-\beta3-\beta4$ and $\beta5-\alpha3-\beta6-\beta7-\beta8$). The two domains are not identical, and one of tham (denoted the first domain hereafter) has an additional short α-helix ($\alpha2$) inserted between $\beta2$ and $\beta3$. In particular, each domain forms a catalytic center with an associated domain from a neighboring protomer. The β-strands ($\beta1-\beta4$) of the first domain associate with the β-strands ($\beta5^*-\beta8^*$) of the second domain from a neighboring subunit in an antiparallel manner, rendering a concave curvature of an eight-stranded β-sheet surrounding the iron center. Another curved eight-stranded β-sheet is formed vice versa, yielding two catalytic iron centers in two β-sheets. $\alpha2$ is situated on the opposite side of the β-sheet, and it completes the cup-shaped active pocket, while two long α-elices ($\alpha1$ and $\alpha3$) closely interact with each other to associate the two domains (Figure 3B). Multiple-sequence alignment of SsDDO with its homologues using Clustal Omega[40] indicates that the secondary structural elements are well conserved (Figure 3C). This arrangement of β-sheets with the formation of a metal binding center from two separate monomers is known for the non-oxidative glyoxalase enzymes but has not been observed in a VOC/type I extradiol dioxygenase.

Nearly every characterized VOC/type I extradiol dioxygenase is of form V architecture, which is a four-module monomer of two back-to-back stacked domains (Figure S1).[9] The well-characterized examples are C23O,[41,42] DHBD,[43,44] and HPCD.[45] To date, the only exceptional scaffold of a deposited VOC dioxygenase is 2,6-dichlorohydroquinone dioxygenase (DCHQD)[46] as a form VI, which is a four-module monomer of two edge-to-edge stacked subunits. Some have speculated that the different topology between DCHQD and the many, characterized, form V VOC dioxygenases might explain how the same VOC scaffold is adapted to oxidatively cleave different classes of hydroxylated aromatic substrates,[13] but the lack of structural data for other scaffolds has limited progress in this area. SsDDO fills a long-standing gap in our understanding by demonstrating that the VOC L-DOPA dioxygenases are of the form IV module arrangement, with an edge-to-edge dimer of back-to-back fused subunits, the first example of its kind from within the VOC/type I extradiol dioxygenase superfamily. These data reveal a previously unrecognized structural class of VOC/type I extradiol dioxygenases, whose structure and mechanism will improve our understanding of the extradiol cleavage reaction.

Metal Coordination. The *de novo* structure of SsDDO shows that the catalytic iron ion is octahedrally coordinated by two histidine residues (His19 and His95*, where an asterisk indicates a residue from a different subunit), a glutamate residue (Glu154*), and three water molecules (Figure 4A). This coordination environment is typical for extradiol dioxygenases across different superfamilies[47] and was first

DOI: 10.1021/acs.biochem.9b00396
Biochemistry 2019, 58, 5339−5350

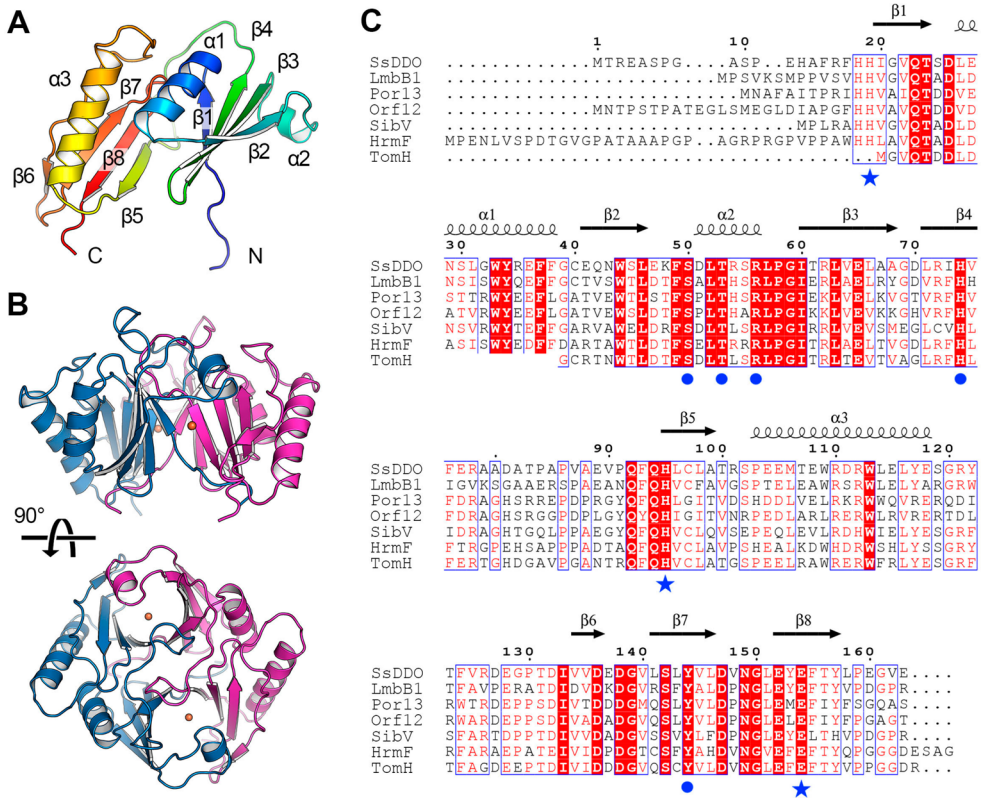

Figure 3. Structural view of the SsDDO monomer and dimer and amino acid sequence alignment of L-DOPA dioxygenases. (A) Monomer structure with labeled secondary structure elements. (B) Two monomers in a dimer colored pink and blue. The active site is formed by dimerization with an iron (orange). (C) Amino acid sequence alignment of SsDDO and its homologues from other *Streptomyces* bacteria. The included sequences are SsDDO from *S. sclerotialus* (WP_051872352), LmbB1 from *S. lincolnensis* (CAA55747), Por13 from *Streptomyces albus* (AEA29636), Orf12 from *Streptomyces refuineus* (ABW71843), SibV from *Streptosporangium sibiricum* (ACN39745), HrmF from *Streptomyces griseoflavus* (AEH41784), and TomH from *Streptomyces achromogenes* (ACN39021). The TomH sequence is truncated relative to those of the other homologues. Highly conserved residues are colored red. Strictly conserved residues are colored white on a red background. The secondary structure elements are defined from the SsDDO structure. Blue stars and circles represent residues involved in the iron coordination and L-DOPA binding site, respectively.

described in the structure of the two-domain VOC enzyme DHBD.[48] The coordinated water molecules interact with second-coordination sphere residues, including His74 and Tyr144*, and other surrounding water molecules. Overall, the catalytic center is located at the interface of two protein molecules in a dimer, and the active site pocket is well-organized with a hydrophobic character, which provides a good cavity for substrate L-DOPA binding. The residues involved in metal binding are strictly conserved among this type of L-DOPA dioxygenases (Figure 3C).

Permutations in sequence caused by gene duplication and domain swapping events somewhere in the evolutionary history of VOC enzymes have made it challenging to identify metal binding residues for this class of one-domain extradiol dioxygenases from sequence alone and resulted in misidentification of Fe binding residues in the past.[7] However, with the increase in the availability of sequences homologous to that of L-DOPA dioxygenase, it is readily apparent that the Fe binding residues identified by the SsDDO structure are conserved across L-DOPA dioxygenases from various organisms. In fact, when SsDDO is superposed with a more distantly related, VOC family protein with a similar topology, such as glyoxalase I (PDB entry 1FA7), the active site and three of the four glyoxalase I metal binding residues are conserved (Figure S4A). Further, the overall structure of SsDDO is quite similar with that of glyoxalase I, which has a *Z* score of 15.8 and a root-mean-square deviation (rmsd) of 1.8 from the result of the DALI search.[49] Glyoxalases are prototypical form IV, VOC family enzymes that use four amino acid ligands (two His and two Glu residues) spread over adjoining $\beta\alpha\beta\beta\beta$ modules to chelate Ni(II), Zn(II), or Cd(II) and catalyze isomerizations,[50,51] highlighting the spatial conservation of residues within the $\beta\alpha\beta\beta\beta$ motif of VOC metal binding enzymes. Nevertheless, molecular replacement using glyoxalase structures was not successful in solving the SsDDO phasing problem during structural determination. Molecular replacement was attempted using the structure of glyoxalase I (PDB entry 1FA7), but phasing was unsuccessful due to weak conservation of sequence between SsDDO and glyoxalase, only 12.5% identity and 24.5% similarity (Figure S4B). While the amino acid sequence level conservation between L-DOPA dioxygenases and other VOC/type I extradiol dioxygenases is low, the evolutionary relationship is apparently preserved at the structural level, as previously found in a similar case between aerobic and anaerobic ribonucleotide reductases.[52]

Crystal Structure of SsDDO in Complex with Its Native Substrate, L-DOPA. The SsDDO and L-DOPA (ES) binary complex crystals were obtained by crystallizing SsDDO under anaerobic conditions and then soaking them with a 5 mM L-DOPA solution. A 2.31 Å resolution data set is shown in Figure 4B. Without fitting any ligand, strong additional density for L-DOPA was observed in the active site. Iterative

DOI: 10.1021/acs.biochem.9b00396
Biochemistry 2019, 58, 5339−5350

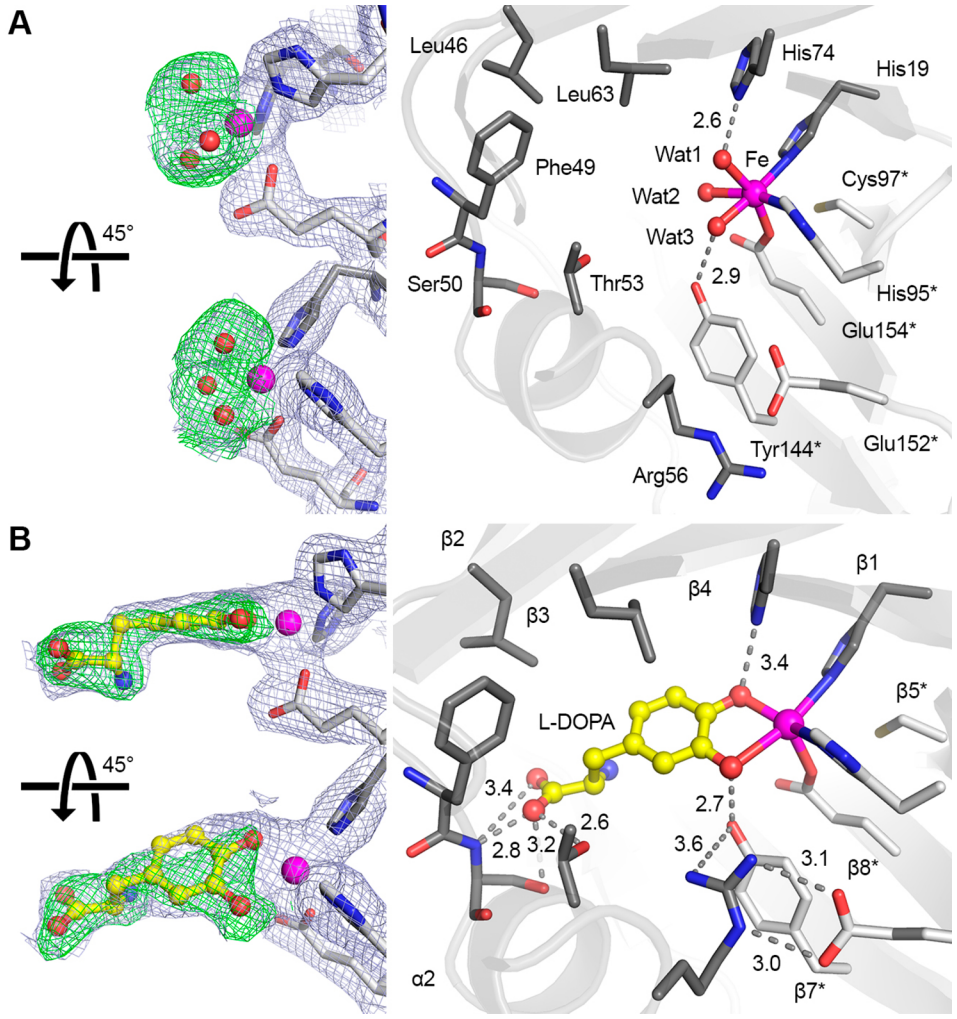

Figure 4. Active site of (A) enzyme only and (B) substrate-bound SsDDO structures. The green $F_o - F_c$ omit map is contoured at 3σ, and the light blue $2F_o - F_c$ electron density map after refinement is contoured at 1σ. Oxygen, nitrogen, and iron atoms are colored red, blue, and magenta, respectively. Carbon atoms from subunit A, subunit B, and L-DOPA are colored white, dark gray, and yellow, respectively. Residues and secondary structural elements with asterisks are from subunit A. Distances between atoms are shown as gray dashed lines.

structural refinements suggest that L-DOPA binds to the iron in a slightly asymmetric, bidentate fashion. An L-DOPA molecule is found coordinated to the iron atom of each of the six subunits with iron−oxygen distances of 2.51 ± 0.03 Å for O1 and 2.45 ± 0.03 Å for O2 Å (subunit E was excluded because its distances failed the Q-test with 90% confidence[53]). These distances are longer and more symmetric than the values of 2.06 and 2.18 Å,[44] 2.0 and 2.4 Å,[54] 1.98 and 2.15 Å,[55] and 2.0 and 2.3 Å[45] reported for other form V and VOC/type I enzymes, respectively. The asymmetric binding of catecholic substrates to extradiol dioxygenase catalytic Fe(II) centers has been interpreted as evidence of ionization at one of the −OH groups of the substrate; that is, the substrate is bound as a monoanion.[54] Previous interpretations of VOC dioxygenase structure assert that the hydroxyl adjacent to the molecular oxygen insertion site (C2−C3 in the case of SsDDO) is deprotonated and has a shorter distance to iron compared to the other oxygen. However, in the case of SsDDO, the opposite is true; the Fe−O1 distance is slightly longer than the Fe−O2 distance in all six subunits (Table S1). To verify our predictions about L-DOPA binding, a different model with a flipped L-DOPA aromatic ring was refined; however, the resulting map missed partial electron density on C5 even though the Fe−O1 distance (2.29 Å) was shorter than the Fe−O2 distance (2.42 Å) (Figure S5). At the current resolution, the model presented in Figure 4B provides a better fit of the observed density, despite the difference in bidentate chelation relative to other characterized VOC extradiol dioxygenases. The different substrate binding mode may be a result of the unique assembly of SsDDO as a form IV VOC dioxygenase.

The stabilization of the substrate oxygen atoms by active site residues has also been well-documented in other VOC/type I enzymes, and in all cases, there is a histidine on one side and a tyrosine on the other, and the aromatic bond adjacent to the tyrosine is cleaved.[54,56] In SsDDO, O1 of the substrate is stabilized by Tyr144* while O2 is stabilized by His74 with distances of 2.7 and 3.4 Å, respectively. In the resting state, these two second-coordination sphere residues initially interact with water ligands (Figure 4A), which are presumably displaced upon substrate binding. The positioning of second-coordination sphere residues once again supports the idea that our current model with C2−C3 facing toward Tyr144* is more appropriate.

In the studies of other extradiol dioxygenases, the same second coordination sphere is also present to assist the asymmetric binding of the substrate and subsequent dioxygen

DOI: 10.1021/acs.biochem.9b00396
Biochemistry 2019, 58, 5339−5350

activation. Additionally, it was proposed that hydrogen bonding from this tyrosine promotes the iron-bound superoxide intermediate to activate the organic substrate and, thus, forms the alkylperoxo intermediate.[12,57] Structural alignment of ES complexes of SsDDO and another well-characterized, form V/two-domain VOC/type I extradiol dioxygenase HPCD indicates that His74 and Tyr144* of SsDDO align well with His200 and Tyr257 of HPCD (Figure S6), respectively. Moreover, the residues known to play critical roles in the extradiol dioxygenase pathway of HPCD and other form V/two-domain VOC/type I extradiol dioxygenases[44,54,56−61] are also found in similar positions.

Notably absent from the SsDDO active site is the putative base that interacts with the active site tyrosine and is proposed to assist in deprotonation of the substrate catechol;[12] this is the role proposed for His248 of HPCD,[57] His246 of C23O,[59] and His241 of DHBD.[54] In SsDDO, there is no such histidine; rather, an arginine (Arg56) occupies the equivalent location. Arg56 is located in short α-helix α2 (Asp51−Arg56) that recognizes the amino acid main chain of the substrate, L-DOPA. The hydroxyl groups of Ser50 and Thr53, as well as the backbone amide of Ser50, also form hydrogen bonding contacts with the carboxylate of L-DOPA (Figure 4B). However, the amino of L-DOPA is surrounded by hydrophobic residues and shows no direct polar interactions with any active site residues. The lack of specific, polar binding determinants for the amino group of L-DOPA could explain why molecules lacking the amino group such as 3,4-dihydroxyphenylacetic acid are substrates of the enzyme.[7]

The overall structure of the ES complex is largely unchanged when compared to the E only structure with an rmsd value of 0.344 Å for 147 C_α atoms; one exception is helix α2, which slightly moves away from the active site to accommodate substrate binding (Figure S7). In particular, Arg56 exhibits a large side chain movement upon substrate binding and is supported by Glu152*. The guanidinium group of Arg56 points away from the active site in the holoenzyme structure (Figure 4A), while it sits over the aromatic ring of Tyr144* in the ES complex, forming a parallel cation−π interaction (Figure 4B). This evidence again supports the hypothesis that Arg56 replaces His248 in HPCD. Moreover, the stabilization of Tyr144* by Arg56 upon substrate binding suggests that the positioning of Tyr144* is critical for substrate recognition and catalysis.

It has been reported that an extradiol dioxygenase employs loop dynamics to accommodate substrates with disparate polarities for rapid enrichment of O_2 at the enzyme active site.[62] The binding of the primary substrate causes conformational changes and results in an increased hydrophobicity in the active site, which subsequently facilitates O_2 enrichment for rapid binding to the iron center. A well-known example is 3-hydroxyanthrinilate 3,4-dioxygenase (HAO), which efficiently catalyzes dioxygenation with a turnover rate of 25 s^{-1} and a k_{cat}/K_M of 1.12 × 10^6 s^{-1} M^{-1}.[62] Interestingly, this phenomenon was not observed in SsDDO by comparing structures with and without L-DOPA, presumably because of a much lower turnover rate of thermophilic SsDDO and a nearly 200-fold smaller k_{cat}/K_M value in the solution. Therefore, the dynamic loop movement is unnecessary for SsDDO to enrich oxygen rapidly.

EPR Characterization of the Non-Heme Ferrous Center. Extradiol dioxygenases have an EPR-silent catalytic Fe(II) center. Therefore, binding of the organic substrate is very often studied by forming a nitrosyl complex with •NO, a spin probe of the EPR-invisible Fe(II) center and an oxygen surrogate.[43,63−65] EPR is sensitive to active site changes upon substrate binding in the solution state, which may be undetectable in the crystal form. By the addition of •NO to reduced SsDDO under anaerobic conditions, a light yellow enzyme−nitrosyl complex (E-NO•) was generated. The corresponding EPR spectrum of E-NO• is characteristic of $S = {}^3/_2$ with resonances at g values of 4.266, 4.101, and 3.939 (Figure 5, trace A), indicative of unresolved signals from at least two E-NO• species. The presence of two species is presumably due to slightly different NO• binding modes in two active sites of one SsDDO dimer. The ES-NO• complex was generated upon addition of the primary substrate L-DOPA, and the resulting EPR spectrum exhibited a predominant species with g values of 4.106 and 3.949 (Figure 5, trace B), suggesting a more homogeneous iron center was formed after binding the organic substrate. The ES-NO• EPR signal was more intense than the E-NO• signal, suggesting NO•, an O_2 surrogate, has a higher affinity for the active iron center after chelation of the organic substrate.

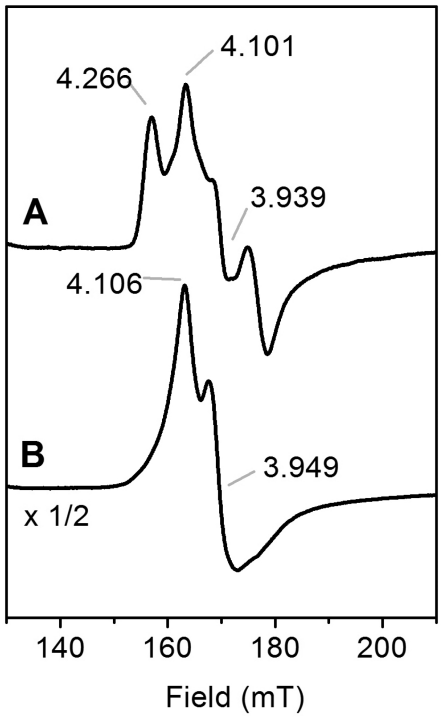

Figure 5. EPR spectra of SsDDO Fe^{II}−nitric oxide complexes. (A) In the absence of substrate, the EPR spectrum of E-NO• is characteristic of at least two $S = {}^3/_2$ species with resonances at g values of 4.266, 4.101, and 3.939. (B) In the presence of the organic substrate, the EPR spectrum of ES-NO• exhibits a more homogeneous iron center with g values of 4.106 and 3.949. The ES-NO• EPR signal is scaled to half-intensity for easy comparison with the E-NO• spectrum. Spectra were collected at a microwave frequency of 9.4 GHz, a modulation frequency of 100 kHz, a modulation amplitude of 6 G, a temperature of 6 K, a microwave power of 0.8 mW, and with an average of four scans.

EPR experiments with extradiol dioxygenases are most often reported with an increased splitting of resonances in the $g = 4$ region, with signals becoming more rhombic after binding of the substrate. For instance, in studies of protocatechuate 2,3-

DOI: 10.1021/acs.biochem.9b00396
Biochemistry 2019, 58, 5339−5350

dioxygenase, upon substrate binding, the resonances changed from g values of 4.11 and 3.95 to g values of 4.21 and 4.85,[43] for protocatechuate 4,5-dioxygenase, resonances changed from g values of 4.09 and 3.91 to g values of 4.21 and 3.77,[66] and in HPCD, resonances changed from g values of 4.04 and 3.96 to g values of 4.12 and 3.87.[67] When compared to these well-studied dioxygenases, the resonances observed for SsDDO did not show the same trend of increased rhombicity upon substrate binding, indicating a less perturbed electron environment. This observation is consistent with our crystallographic data, which revealed the substrate Fe−O distances were longer and more symmetric than for other prototypical extradiol dioxygenases and may indicate that DOPA binds to SsDDO as a diol rather than a monoanion. It should be noted that both E-NO$^{\bullet}$ and ES-NO$^{\bullet}$ complexes exhibited an $S = {}^{1}/_{2}$ dinitrosyl signal in the $g = 2$ region caused by excess $^{\bullet}$NO (Figure S8) which was unaffected by the addition of L-DOPA. The dinitrosyl signal has been observed in synthetic compounds and some non-heme iron proteins; however, it is rarely observed in extradiol dioxygenases.[68−71] The observed dinitrosyl species indicates that the solvent-derived ligands bind the iron center much more weakly than other extradiol dioxygenases and that the active site has more flexibility, allowing the diatomic gas to easily replace the water ligands.

CONCLUDING REMARKS

Cleavage of an aromatic ring with the controlled insertion of molecular oxygen is one of nature's most elegant reactions. The VOC/type I extradiol dioxygenase superfamily is a collection of prototypical catechol-cleaving enzymes. This superfamily, first defined by catechol-2,3-dioxygenase, has grown to include the example discussed in this work, L-DOPA dioxygenase. L-DOPA dioxygenase proteins are present in biosynthetic pathways that yield antibacterial or antitumor natural products. A new L-DOPA dioxygenase, SsDDO, was identified, sequenced, and biochemically and structurally characterized. The *de novo* crystal structures of both the resting state and the ES complex were determined at high resolution. Together, these results represent the first comprehensive structural study of an L-DOPA dioxygenase and suggest that the substrate binding is significantly altered compared to that of other extradiol dioxygenases. The global structure indicates SsDDO is novel among VOC/type I extradiol dioxygenases, an edge-to-edge dimer of back-to-back fused subunits from one domain (form IV). When compared to other structurally characterized VOC/type I extradiol dioxygenases (form V), the active site second-coordination sphere residues playing essential catalytic roles are spatially well-conserved in SsDDO. The only exception is a histidine, often present to assist the deprotonation of the substrate catechol, is replaced in SsDDO with an arginine that undergoes significant movement upon substrate binding. However, in marked contrast to structurally characterized VOC/type I extradiol dioxygenases such as catechol 2,3-dioxygenase, SsDDO forms its active site by dimerization of individual monomers, a topology thus far unprecedented among extradiol dioxygenases of the VOC superfamily. These findings promise to provide new insights into the relationship between VOC domain architecture and enzymatic function.

ASSOCIATED CONTENT

Supporting Information

The Supporting Information is available free of charge on the ACS Publications website at DOI: 10.1021/acs.biochem.9b00396.

Table S1 and Figures S1−S8 (PDF)

Accession Codes

SsDDO: gene accession number MK873432, protein accession number QCR99238.

AUTHOR INFORMATION

Corresponding Authors

*E-mail: Feradical@utsa.edu. Telephone: +1-210-458-7062.
*E-mail: colabroy@muhlenberg.edu. Telephone: +1-484-664-3665.

ORCID

Aimin Liu: 0000-0002-4182-8176

Author Contributions

K.L.C. and Y.F. identified the SsDDO gene, performed the cloning, and demonstrated the catalytic activity. Y.W. conducted the SsDDO sequence similarity network study and the temperature-dependent kinetic assays. Y.W. and I.S. determined the X-ray crystal structures with Y.F. participating in the initial crystallization and data collection. Y.W. and K.L.C. prepared the initial draft with A.L.'s input. All authors approved the final draft.

Funding

The work is supported by National Science Foundation Grants CHE-1808637 (to A.L.) and CHE-1708237 (to K.L.C.) and in part by National Institutes of Health Grant R01GM107529 and the Lutcher Brown Endowment (to A.L.).

Notes

The authors declare no competing financial interest.

ACKNOWLEDGMENTS

The authors thank Mr. Ian Davis for assistance in acquiring the EPR data and revising the manuscript. X-ray diffraction data were collected at synchrotron beamline 19-BM of the Structural Biology Center (SBC) at the Advanced Photon Source of Argonne National Laboratory under the user program GUP 48198 and beamline BL9-2 of the Stanford Synchrotron Radiation Lightsource (SSRL) under user program 5B14, SLAC National Accelerator Laboratory. SBC-CAT is operated by UChicago Argonne, LLC, for the U.S. Department of Energy, Office of Biological and Environmental Research, under Contract DE-AC02-06CH11357. Use of the Stanford Synchrotron Radiation Lightsource, SLAC National Accelerator Laboratory, is supported by the U.S. Department of Energy, Office of Science, Office of Basic Energy Sciences, under Contract DE-AC02-76SF00515.

REFERENCES

(1) Bugg, T. D., Ahmad, M., Hardiman, E. M., and Singh, R. (2011) The emerging role for bacteria in lignin degradation and bio-product formation. *Curr. Opin. Biotechnol. 22* (3), 394−400.

(2) Kamimura, N., Takahashi, K., Mori, K., Araki, T., Fujita, M., Higuchi, Y., and Masai, E. (2017) Bacterial catabolism of lignin-derived aromatics: New findings in a recent decade: Update on bacterial lignin catabolism. *Environ. Microbiol. Rep. 9* (6), 679−705.

(3) Wu, W., Dutta, T., Varman, A. M., Eudes, A., Manalansan, B., Loque, D., and Singh, S. (2017) Lignin valorization: Two hybrid

DOI: 10.1021/acs.biochem.9b00396
Biochemistry 2019, 58, 5339−5350

biochemical routes for the conversion of polymeric lignin into value-added chemicals. *Sci. Rep. 7* (1), 8420.
(4) Hayaishi, O., and Hashimoto, K. (1950) Pyrocatecase - a new enzyme catalizing oxidative breakdown of pyrocatechin. *J. Biochem. 37* (3), 371−374.
(5) Vaillancourt, F. H., Bolin, J. T., and Eltis, L. D. (2006) The ins and outs of ring-cleaving dioxygenases. *Crit. Rev. Biochem. Mol. Biol. 41* (4), 241−267.
(6) Chen, Y. L., Yu, C. P., Lee, T. H., Goh, K. S., Chu, K. H., Wang, P. H., Ismail, W., Shih, C. J., and Chiang, Y. R. (2017) Biochemical mechanisms and catabolic enzymes involved in bacterial estrogen degradation pathways. *Cell Chem. Biol. 24* (6), 712−724.
(7) Colabroy, K. L., Hackett, W. T., Markham, A. J., Rosenberg, J., Cohen, D. E., and Jacobson, A. (2008) Biochemical characterization of L-DOPA 2,3-dioxygenase, a single-domain type I extradiol dioxygenase from lincomycin biosynthesis. *Arch. Biochem. Biophys. 479* (2), 131−138.
(8) Zhang, Y., Colabroy, K. L., Begley, T. P., and Ealick, S. E. (2005) Structural studies on 3-hydroxyanthranilate-3,4-dioxygenase: the catalytic mechanism of a complex oxidation involved in NAD biosynthesis. *Biochemistry 44* (21), 7632−7643.
(9) He, P., and Moran, G. R. (2011) Structural and mechanistic comparisons of the metal-binding members of the vicinal oxygen chelate (VOC) superfamily. *J. Inorg. Biochem. 105* (10), 1259−1272.
(10) Barry, K. P., and Taylor, E. A. (2013) Characterizing the promiscuity of LigAB, a lignin catabolite degrading extradiol dioxygenase from *Sphingomonas paucimobilis* SYK-6. *Biochemistry 52* (38), 6724−6736.
(11) Fetzner, S. (2012) Ring-cleaving dioxygenases with a cupin fold. *Appl. Environ. Microbiol. 78* (8), 2505−2514.
(12) Lipscomb, J. D. (2008) Mechanism of extradiol aromatic ring-cleaving dioxygenases. *Curr. Opin. Struct. Biol. 18* (6), 644−649.
(13) Meng, E. C., and Babbitt, P. C. (2011) Topological variation in the evolution of new reactions in functionally diverse enzyme superfamilies. *Curr. Opin. Struct. Biol. 21* (3), 391−397.
(14) Bergdoll, M., Eltis, L. D., Cameron, A. D., Dumas, P., and Bolin, J. T. (1998) All in the family: Structural and evolutionary relationships among three modular proteins with diverse functions and variable assembly. *Protein Sci. 7* (8), 1661−1670.
(15) Peschke, U., Schmidt, H., Zhang, H. Z., and Piepersberg, W. (1995) Molecular characterization of the lincomycin-production gene cluster of *Streptomyces lincolnensis* 78−11. *Mol. Microbiol. 16* (6), 1137−1156.
(16) Neusser, D., Schmidt, H., Spizek, J., Novotna, J., Peschke, U., Kaschabeck, S., Tichy, P., and Piepersberg, W. (1998) The genes *lmbB1* and *lmbB2* of *Streptomyces lincolnensis* encode enzymes involved in the conversion of L-tyrosine to propylproline during the biosynthesis of the antibiotic lincomycin A. *Arch. Microbiol. 169* (4), 322−332.
(17) Novotna, J., Honzatko, A., Bednar, P., Kopecky, J., Janata, J., and Spizek, J. (2004) L-3,4-Dihydroxyphenyl alanine-extradiol cleavage is followed by intramolecular cyclization in lincomycin biosynthesis. *Eur. J. Biochem. 271* (18), 3678−3683.
(18) Zhong, G., Zhao, Q., Zhang, Q., and Liu, W. (2017) 4-Alkyl-L-(dehydro)proline biosynthesis in actinobacteria involves N-terminal nucleophile-hydrolase activity of gamma-glutamyltranspeptidase homolog for C-C bond cleavage. *Nat. Commun. 8*, 16109.
(19) Hofer, I., Crusemann, M., Radzom, M., Geers, B., Flachshaar, D., Cai, X., Zeeck, A., and Piel, J. (2011) Insights into the biosynthesis of hormaomycin, an exceptionally complex bacterial signaling metabolite. *Chem. Biol. 18* (3), 381−391.
(20) Hu, Y., Phelan, V., Ntai, I., Farnet, C. M., Zazopoulos, E., and Bachmann, B. O. (2007) Benzodiazepine biosynthesis in *Streptomyces refuineus*. *Chem. Biol. 14* (6), 691−701.
(21) Saha, S., Li, W., Gerratana, B., and Rokita, S. E. (2015) Identification of the dioxygenase-generated intermediate formed during biosynthesis of the dihydropyrrole moiety common to anthramycin and sibiromycin. *Bioorg. Med. Chem. 23* (3), 449−454.
(22) Najmanova, L., Ulanova, D., Jelinkova, M., Kamenik, Z., Kettnerova, E., Koberska, M., Gazak, R., Radojevic, B., and Janata, J. (2014) Sequence analysis of porothramycin biosynthetic gene cluster. *Folia Microbiol. (Dordrecht, Neth.) 59* (6), 543−552.
(23) Li, W., Khullar, A., Chou, S., Sacramo, A., and Gerratana, B. (2009) Biosynthesis of sibiromycin, a potent antitumor antibiotic. *Appl. Environ. Microbiol. 75* (9), 2869−2878.
(24) Li, W., Chou, S., Khullar, A., and Gerratana, B. (2009) Cloning and characterization of the biosynthetic gene cluster for tomaymycin, an SJG-136 monomeric analog. *Appl. Environ. Microbiol. 75* (9), 2958−2963.
(25) Colabroy, K. L., Smith, I. R., Vlahos, A. H., Markham, A. J., and Jakubik, M. E. (2014) Defining a kinetic mechanism for L-DOPA 2,3-dioxygenase, a single-domain type I extradiol dioxygenase from *Streptomyces lincolnensis*. *Biochim. Biophys. Acta, Proteins Proteomics 1844* (3), 607−614.
(26) Shin, I., Han, K., and Rhee, S. (2014) Structural insights into the substrate specificity of (s)-ureidoglycolate amidohydrolase and its comparison with allantoate amidohydrolase. *J. Mol. Biol. 426* (17), 3028−3040.
(27) Liu, F., Geng, J., Gumpper, R. H., Barman, A., Davis, I., Ozarowski, A., Hamelberg, D., and Liu, A. (2015) An iron reservoir to the catalytic metal: the rubredoxin iron in an extradiol dioxygenase. *J. Biol. Chem. 290* (25), 15621−15634.
(28) Davis, M. D., Kaufman, S., and Milstien, S. (1986) A modified ferrozine method for the measurement of enzyme-bound iron. *J. Biochem. Biophys. Methods 13* (1), 39−45.
(29) Otwinowski, Z., and Minor, W. (1997) Processing of X-ray diffraction data collected in oscillation mode. *Methods Enzymol. 276*, 307−326.
(30) Terwilliger, T. C., Adams, P. D., Read, R. J., McCoy, A. J., Moriarty, N. W., Grosse-Kunstleve, R. W., Afonine, P. V., Zwart, P. H., and Hung, L. W. (2009) Decision-making in structure solution using Bayesian estimates of map quality: the PHENIX AutoSol wizard. *Acta Crystallogr., Sect. D: Biol. Crystallogr. 65* (Part 6), 582−601.
(31) Terwilliger, T. C., Grosse-Kunstleve, R. W., Afonine, P. V., Moriarty, N. W., Zwart, P. H., Hung, L. W., Read, R. J., and Adams, P. D. (2008) Iterative model building, structure refinement and density modification with the PHENIX Auto Build wizard. *Acta Crystallogr., Sect. D: Biol. Crystallogr. 64* (Part 1), 61−69.
(32) Adams, P. D., Grosse-Kunstleve, R. W., Hung, L. W., Ioerger, T. R., McCoy, A. J., Moriarty, N. W., Read, R. J., Sacchettini, J. C., Sauter, N. K., and Terwilliger, T. C. (2002) PHENIX: building new software for automated crystallographic structure determination. *Acta Crystallogr., Sect. D: Biol. Crystallogr. 58* (Part 11), 1948−1954.
(33) Strong, M., Sawaya, M. R., Wang, S., Phillips, M., Cascio, D., and Eisenberg, D. (2006) Toward the structural genomics of complexes: crystal structure of a PE/PPE protein complex from Mycobacterium tuberculosis. *Proc. Natl. Acad. Sci. U. S. A. 103* (21), 8060−8065.
(34) Wang, Y., Davis, I., Shin, I., Wherritt, D. J., Griffith, W. P., Dornevil, K., Colabroy, K. L., and Liu, A. (2019) Biocatalytic carbon−hydrogen and carbon−fluorine bond cleavage through hydroxylation promoted by a histidyl-ligated heme enzyme. *ACS Catal. 9* (6), 4764−4776.
(35) Hurley, L. H., Lasswell, W. L., Ostrander, J. M., and Parry, R. (1979) Pyrrolo[1,4]benzodiazepine antibiotics. Biosynthetic conversion of tyrosine to the C2- and C3-proline moieties of anthramycin, tomaymycin, and sibiromycin. *Biochemistry 18* (19), 4230−4237.
(36) Zhang, D., Tang, Z., and Liu, W. (2018) Biosynthesis of lincosamide antibiotics: reactions associated with degradation and detoxification pathways play a constructive role. *Acc. Chem. Res. 51* (6), 1496−1506.
(37) Yadav, A. K., Vardhan, S., Yandigeri, M. S., Srivastava, A. K., and Arora, D. K. (2011) Optimization of keratin degrading enzyme from thermophillic strain of *Streptomyces sclerotialus*. *Res. J. Microbiol. 6* (9), 693−705.

DOI: 10.1021/acs.biochem.9b00396
Biochemistry 2019, 58, 5339−5350

(38) Doroghazi, J. R., Albright, J. C., Goering, A. W., Ju, K. S., Haines, R. R., Tchalukov, K. A., Labeda, D. P., Kelleher, N. L., and Metcalf, W. W. (2014) A roadmap for natural product discovery based on large-scale genomics and metabolomics. *Nat. Chem. Biol. 10* (11), 963−968.
(39) Gerlt, J. A., Bouvier, J. T., Davidson, D. B., Imker, H. J., Sadkhin, B., Slater, D. R., and Whalen, K. L. (2015) Enzyme function initiative-enzyme similarity tool (EFI-EST): A web tool for generating protein sequence similarity networks. *Biochim. Biophys. Acta, Proteins Proteomics 1854* (8), 1019−1037.
(40) Sievers, F., Wilm, A., Dineen, D., Gibson, T. J., Karplus, K., Li, W., Lopez, R., McWilliam, H., Remmert, M., Soding, J., Thompson, J. D., and Higgins, D. G. (2011) Fast, scalable generation of high-quality protein multiple sequence alignments using Clustal Omega. *Mol. Syst. Biol. 7*, 539.
(41) Lee, J., Oh, J., Min, K. R., Kim, C. K., Min, K. H., Lee, K. S., Kim, Y. C., Lim, J. Y., and Kim, Y. (1996) Structure of catechol 2,3-dioxygenase gene encoded in chromosomal DNA of *Pseudomonas putida* KF715. *Biochem. Biophys. Res. Commun. 224* (3), 831−836.
(42) Winkler, J., Eltis, L. D., Dwyer, D. F., and Rohde, M. (1995) Tetrameric structure and cellular location of catechol 2,3-dioxygenase. *Arch. Microbiol. 163* (1), 65−69.
(43) Eltis, L. D., Hofmann, B., Hecht, H. J., Lunsdorf, H., and Timmis, K. N. (1993) Purification and crystallization of 2,3-dihydroxybiphenyl 1,2-dioxygenase. *J. Biol. Chem. 268* (4), 2727−2732.
(44) Uragami, Y., Senda, T., Sugimoto, K., Sato, N., Nagarajan, V., Masai, E., Fukuda, M., and Mitsui, Y. (2001) Crystal structures of substrate free and complex forms of reactivated BphC, an extradiol type ring-cleavage dioxygenase. *J. Inorg. Biochem. 83* (4), 269−279.
(45) Vetting, M. W., Wackett, L. P., Que, L., Jr., Lipscomb, J. D., and Ohlendorf, D. H. (2004) Crystallographic comparison of manganese- and iron-dependent homoprotocatechuate 2,3-dioxygenases. *J. Bacteriol. 186* (7), 1945−1958.
(46) Hayes, R. P., Green, A. R., Nissen, M. S., Lewis, K. M., Xun, L., and Kang, C. (2013) Structural characterization of 2,6-dichloro-p-hydroquinone 1,2-dioxygenase (PcpA) from *Sphingobium chlorophenolicum*, a new type of aromatic ring-cleavage enzyme. *Mol. Microbiol. 88* (3), 523−536.
(47) Wang, Y., Li, J., and Liu, A. (2017) Oxygen activation by mononuclear nonheme iron dioxygenases involved in the degradation of aromatics. *J. Biol. Inorg. Chem. 22* (2−3), 395−405.
(48) Han, S., Eltis, L. D., Timmis, K. N., Muchmore, S. W., and Bolin, J. T. (1995) Crystal structure of the biphenyl-cleaving extradiol dioxygenase from a PCB-degrading pseudomonad. *Science 270* (5238), 976−980.
(49) Holm, L., and Sander, C. (1995) Dali: a network tool for protein structure comparison. *Trends Biochem. Sci. 20* (11), 478−480.
(50) Ariza, A., Vickers, T. J., Greig, N., Armour, K. A., Dixon, M. J., Eggleston, I. M., Fairlamb, A. H., and Bond, C. S. (2006) Specificity of the trypanothione-dependent *Leishmania* major glyoxalase I: structure and biochemical comparison with the human enzyme. *Mol. Microbiol. 59* (4), 1239−1248.
(51) He, M. M., Clugston, S. L., Honek, J. F., and Matthews, B. W. (2000) Determination of the structure of *Escherichia coli* glyoxalase I suggests a structural basis for differential metal activation. *Biochemistry 39* (30), 8719−8727.
(52) Logan, D. T., Andersson, J., Sjöberg, B. M., and Nördlund, P. (1999) A glycyl radical site in the crystal structure of a class III ribonucleotide reductase. *Science (Washington, DC, U. S.) 283* (5407), 1499−1504.
(53) Rorabacher, D. B. (1991) Statistical treatment for rejection of deviant values - critical values of Dixon's "Q" parameter and related subrange ratios at the 95% confidence level. *Anal. Chem. 63* (2), 139−146.
(54) Vaillancourt, F. H., Barbosa, C. J., Spiro, T. G., Bolin, J. T., Blades, M. W., Turner, R. F., and Eltis, L. D. (2002) Definitive evidence for monoanionic binding of 2,3-dihydroxybiphenyl to 2,3-dihydroxybiphenyl 1,2-dioxygenase from UV resonance Raman spectroscopy, UV/Vis absorption spectroscopy, and crystallography. *J. Am. Chem. Soc. 124* (11), 2485−2496.
(55) Sato, N., Uragami, Y., Nishizaki, T., Takahashi, Y., Sazaki, G., Sugimoto, K., Nonaka, T., Masai, E., Fukuda, M., and Senda, T. (2002) Crystal structures of the reaction intermediate and its homologue of an extradiol-cleaving catecholic dioxygenase. *J. Mol. Biol. 321* (4), 621−636.
(56) Cho, H. J., Kim, K., Sohn, S. Y., Cho, H. Y., Kim, K. J., Kim, M. H., Kim, D., Kim, E., and Kang, B. S. (2010) Substrate binding mechanism of a type I extradiol dioxygenase. *J. Biol. Chem. 285* (45), 34643−34652.
(57) Kovaleva, E. G., and Lipscomb, J. D. (2012) Structural basis for the role of tyrosine 257 of homoprotocatechuate 2,3-dioxygenase in substrate and oxygen activation. *Biochemistry 51* (44), 8755−8763.
(58) Emerson, J. P., Wagner, M. L., Reynolds, M. F., Que, L., Jr., Sadowsky, M. J., and Wackett, L. P. (2005) The role of histidine 200 in MndD, the Mn(II)-dependent 3,4-dihydroxyphenylacetate 2,3-dioxygenase from *Arthrobacter globiformis* CM-2, a site-directed mutagenesis study. *J. Biol. Inorg. Chem. 10* (7), 751−760.
(59) Viggiani, A., Siani, L., Notomista, E., Birolo, L., Pucci, P., and Di Donato, A. (2004) The role of the conserved residues His-246, His-199, and Tyr-255 in the catalysis of catechol 2,3-dioxygenase from *Pseudomonas stutzeri* OX1. *J. Biol. Chem. 279* (47), 48630−48639.
(60) Kovaleva, E. G., Rogers, M. S., and Lipscomb, J. D. (2015) Structural basis for substrate and oxygen activation in homoprotocatechuate 2,3-dioxygenase: roles of conserved active site histidine 200. *Biochemistry 54* (34), 5329−5339.
(61) Groce, S. L., and Lipscomb, J. D. (2005) Aromatic ring cleavage by homoprotocatechuate 2,3-dioxygenase: role of His200 in the kinetics of interconversion of reaction cycle intermediates. *Biochemistry 44* (19), 7175−7188.
(62) Yang, Y., Liu, F., and Liu, A. (2018) Adapting to oxygen: 3-Hydroxyanthrinilate 3,4-dioxygenase employs loop dynamics to accommodate two substrates with disparate polarities. *J. Biol. Chem. 293* (27), 10415−10424.
(63) Emerson, J. P., Kovaleva, E. G., Farquhar, E. R., Lipscomb, J. D., and Que, L., Jr. (2008) Swapping metals in Fe- and Mn-dependent dioxygenases: evidence for oxygen activation without a change in metal redox state. *Proc. Natl. Acad. Sci. U. S. A. 105* (21), 7347−7352.
(64) Orville, A. M., and Lipscomb, J. D. (1993) Simultaneous binding of nitric oxide and isotopically labeled substrates or inhibitors by reduced protocatechuate 3,4-dioxygenase. *J. Biol. Chem. 268* (12), 8596−8607.
(65) Yan, F., Moon, S. J., Liu, P., Zhao, Z., Lipscomb, J. D., Liu, A., and Liu, H. W. (2007) Determination of the substrate binding mode to the active site iron of (S)-2-hydroxypropylphosphonic acid epoxidase using ^{17}O-enriched substrates and substrate analogues. *Biochemistry 46* (44), 12628−12638.
(66) Arciero, D. M., Lipscomb, J. D., Huynh, B. H., Kent, T. A., and Münck, E. (1983) EPR and Mössbauer studies of protocatechuate 4,5-dioxygenase. Characterization of a new Fe^{2+} environment. *J. Biol. Chem. 258* (24), 14981−14991.
(67) Miller, M. A., and Lipscomb, J. D. (1996) Homoprotocatechuate 2,3-dioxygenase from Brevibacterium fuscum. A dioxygenase with catalase activity. *J. Biol. Chem. 271* (10), 5524−5535.
(68) Orville, A. M., Chen, V. J., Kriauciunas, A., Harpel, M. R., Fox, B. G., Münck, E., and Lipscomb, J. D. (1992) Thiolate ligation of the active site Fe^{2+} of isopenicillin *N* synthase derives from substrate rather than endogenous cysteine: spectroscopic studies of site-specific Cys'Ser mutated enzymes. *Biochemistry 31* (19), 4602−4612.
(69) Jo, D. H., Chiou, Y. M., and Que, L., Jr. (2001) Models for extradiol cleaving catechol dioxygenases: syntheses, structures, and reactivities of iron(II)-monoanionic catecholate complexes. *Inorg. Chem. 40* (13), 3181−3190.
(70) Tinberg, C. E., Tonzetich, Z. J., Wang, H., Do, L. H., Yoda, Y., Cramer, S. P., and Lippard, S. J. (2010) Characterization of iron dinitrosyl species formed in the reaction of nitric oxide with a biological Rieske center. *J. Am. Chem. Soc. 132* (51), 18168−18176.

DOI: 10.1021/acs.biochem.9b00396
Biochemistry 2019, 58, 5339−5350

(71) Li, J., Koto, T., Davis, I., and Liu, A. (2019) Probing the Cys-Tyr cofactor biogenesis in cysteine dioxygenase by the genetic incorporation of fluorotyrosine. *Biochemistry 58* (17), 2218−2227.

DOI: 10.1021/acs.biochem.9b00396
Biochemistry 2019, 58, 5339−5350